Supplementary information

XPS experimental and DFT investigations of solid solutions $Mo_{1-x}Re_xS_2$ (0<x<0.20)

*Svetlana A. Dalmatova [a,c], Anastasiya D. Fedorenko[a], Lev N. Mazalov[a,c], Igor P. Asanov[a,c], Alexandra Yu. Ledneva[a], Mariya S. Tarasenko[a], Andrey N. Enyashin[b], Vladimir I. Zaikovskii[d] and Vladimir E. Fedorov[a,c]**

[a] *Nikolaev Institute of Inorganic Chemistry, Siberian Branch of the Russian Academy of Sciences, Prospect Acad. Lavrentieva, 3, Novosibirsk 630090, Russia*
[b] *Institute of Solid State Chemistry, Ural Branch of the Russian Academy of Sciences, Pervomayskaya Str., 91, Ekaterinburg 620990, Russia*
[c] *Novosibirsk State University, Pirogova 2, Novosibirsk 630090 Russia*
[d] *Boreskov Institute of Catalysis Siberian Branch of the Russian Academy of Sciences, Prospect Acad. Lavrentieva, 5, Novosibirsk 630090, Russia*

** fed@niic.nsc.ru*

Starting stoichiometry	EDS analysis
MoS_2	$Mo_{0.99}S_2$
$Mo_{0.95}Re_{0.05}S_2$	$Mo_{0.94}Re_{0.04}S_2$
$Mo_{0.9}Re_{0.1}S_2$	$Mo_{0.91}Re_{0.08}S_2$
$Mo_{0.85}Re_{0.15}S_2$	$Mo_{0.87}Re_{0.16}S_2$
$Mo_{0.80}Re_{0.20}S_2$	$Mo_{0.81}Re_{0.22}S_2$
ReS_2	$Re_{1.01}S_2$

Table S1. Synthetic stoichiometry and EDS elemental analysis data for the synthesized samples $Mo_{1-x}Re_xS_2$ (x = 0, 0.05, 0.10, 0.15and 0.20)

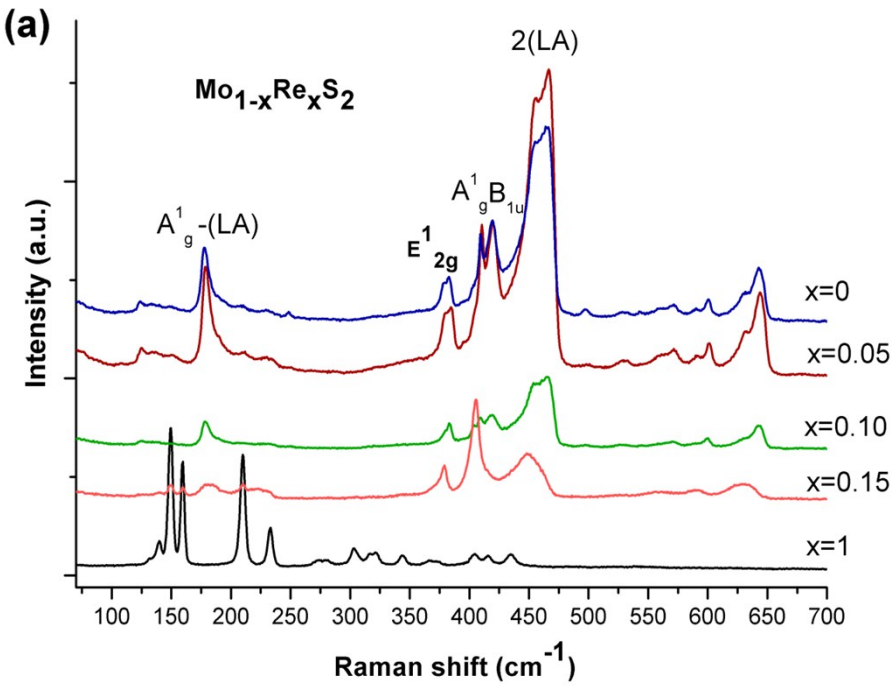

Figure S1. Raman-spectra of $Mo_{1-x}Re_xS_2$(x = 0, 0.05, 0.10 and 0.15). LA corresponds to second-order process involving the longitudinal acoustic phonons.

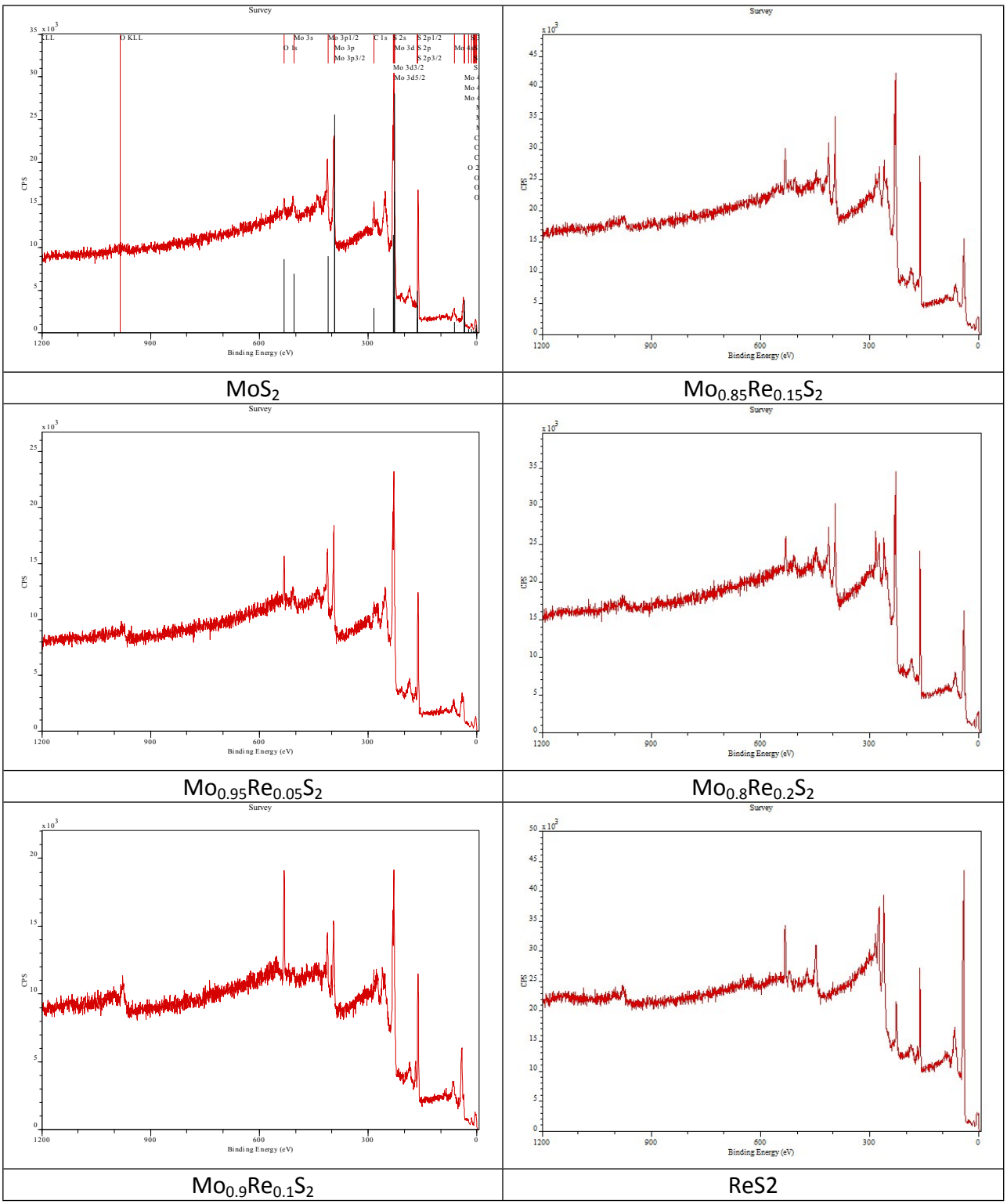

Figure S2. XPS spectra of pristine MoS_2, ReS_2 and $Mo_{1-x}Re_xS_2$ solid solutions, x= 0.05, 0.1, 0.15, 0.2

	Mo3$d_{5/2}$				S2$p_{3/2}$				Re4$f_{7/2}$			
Compound		E_b, eV	S, %	Type of atom		E_b eV	S, %	Type of atom		E_b, eV	S, %	Type of atom
MoS_2	(I)	229,6	100	Mo1[a]	(0)	163,8	3,3	$(S\text{-}S)^{2-}$			-	
					(I)	162,4	96,7	S1[c]				
$Mo_{0,95}Re_{0,05}S_2$	(I)	229,6	75,4	Mo1	(I)	162,5	69,3	S1	(I)	41,4	100	Re1[e]
	(II)	229,1	24,6	Mo2[b]	(II)	162	22,4	S2[d]				
					(III)	168,7	7,1	SO_4^{2-}				
					(IV)	161	1,1	1T MoS_2				
$Mo_{0,9}Re_{0,1}S_2$	(I)	229,6	54,3	Mo1	(I)	162,5	49,7	S1	(I)	41,4	100	Re1
	(II)	229,2	45,7	Mo2	(II)	161,9	31,7	S2				
					(III)	168,7	15,5	SO_4^{2-}				
					(IV)	161	3,1	1T MoS_2				
$Mo_{0,85}Re_{0,15}S_2$	(I)	229,6	55,1	Mo1	(0)	163,4	3,8	$(S\text{-}S)^{2-}$	(I)	41,2	60,1	Re1
	(II)	229,4	42,2	Mo2	(I)	162,4	68,1	S1	(II)	42,3	30,8	ReO_2
	(III)	233	2,7	MoO_x	(II)	161,7	11,9	S2	(III)	41,6	9,1	Re2[f]
					(III)	168,5	4,4	SO_4^{2-}				
					(IV)	161,2	9,3	1T MoS_2				
					(V)	166,6	2,5	SO_3^{2-}				
$Mo_{0,8}Re_{0.2}S_2$	(I)	229,6	57,3	Mo1	(I)	162,3	85	S1	(I)	41,4	63,8	Re1
	(II)	229,3	40,5	Mo2	(II)	161,4	4,2	S2	(II)	42,6	7,3	ReO2
	(III)	233,3	2,2	MoO_x	(III)	168	10,8	SO_4^{2-}	(III)	41,8	28,9	Re2
ReS_2			-		(I)	162,6	54,3	S1	(I)	42,1	84,3	Re1
					(II)	161,9	36,9	ReS2 metal	(II)	43,2	2,9	ReO_2
					(III)	168,9	8,8	SO_4^{2-}	(IV)	41,5	12,8	ReS2 metal

Table S2. The values of the binding energies and integral intensities for MoS_2, ReS_2 and $Mo_{1-x}Re_xS_2$ solid solutions, x= 0.05, 0.1, 0.15, 0.2.

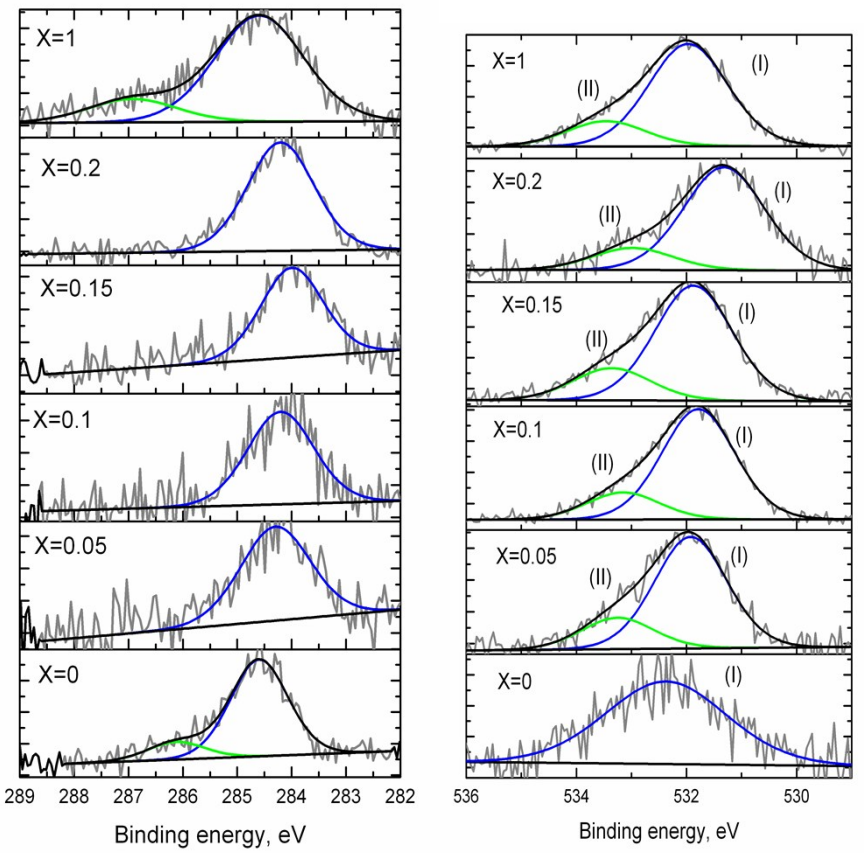

Figure S3. C1s (a) and O1s (b) XPS spectra of $Mo_{1-x}Re_xS_2$

O*1s*				C*1s*				
Compound	E_b, eV		S, %	Type of atom	E_b, eV		S, %	Type of atom
MoS_2	(I) O1s	532.4	100	C-O	(I) C1s (II) C1s	284.6 286.1	84,6 15,4	C-C C-O
$Mo_{0.95}Re_{0.05}S_2$	(I) O1s (II) O1s	531,9 533.3	78,1 21,9	C-O SO_4^{2-}	(I) C1s	284.3	100	C-C
$Mo_{0.9}Re_{0.1}S_2$	(I) O1s (II) O1s	531,8 533.3	80,3 19,7	C-O SO_4^{2-}	(I) C1s	284.2	100	C-C
$Mo_{0,85}Re_{0.15}S_2$	(I) O1s (II) O1s	531,1 532,6	78,2 21,8	C-O SO_4^{2-}	(I) C1s	284.5	100	C-C
$Mo_{0,8}Re_{0.2}S_2$	(I) O1s (II) O1s	531,3 533,0	82,4 17,6	C-O SO_4^{2-}	(I) C1s	284,2	100	C-C
ReS2	(I) O1s (II) O1s	532,0 533.5	80,1 19,9	C-O SO_4^{2-}	(I) C1s (II) C1s	284.6 286.9	81,9 18,1	C-C

Table S3. The values of the binding energies E_b and integral intensities S of the C*1s* and O*1s* XPS spectra

The S2*p* (0) component appearing in pure MoS_2 and associated with the formation of defect structures or S_2^{2-}groups disappears in the samples after doping. The distance between S^{2-}(S(I)) and $(S\text{-}S)^{2-}$(S(0)) is in good agreement with literature [1]. In addition, S2*p* (~ 1%) (IV) component appears in the S2*p* spectrum after doping with rhenium atoms. This component can be considered as contribution of structural defects or disordered structure close to the metastable 1T-MoS_2 octahedral configuration locally formed during doping. Since rhenium disulfide crystallizes in another structural type than MoS_2, the replacement of Mo by Re in the MoS_2 lattice may lead to the destabilization of the 2H-MoS_2 phase. Also, S2p (III) component corresponding to SO_4^{2-} appears after doping. We suppose that SO_4^{2-} functionalizes the edges of the MoS_2 layers [2]. In the sample with x=0.15, a small amount of SO_3^{2-}, ReO_2 and [3], MoO_x, were observed (S2p(V)), which is caused by the oxidation of samples in atmospheric environment [4].

1. Lince, J.R., et al., *Chemical Effects of Ne+ Bombardment on the MoS_2(0001) Surface Studied by High-Resolution Photoelectron-Spectroscopy.* Surface Science, 1989. **210**(3): p. 387-405.
2. Krasnov, A.P., et al., *Effect of particle size and composition of powdered nanocrystalline molybdenum disulfide on its tribological behavior.* Journal of Friction and Wear, 2014. **35**(4): p. 330-338.
3. Aliaga, J.A., et al., *Synthesis of highly destacked ReS2 layers embedded in amorphous carbon from a metal-organic precursor.* Journal of Non-Crystalline Solids, 2016. **447**: p. 29-34.
4. Santos, L.V., et al., *Diamond-like-carbon and molybdenum disulfide nanotribology studies using atomic force measurements.* Diamond and Related Materials, 2001. **10**(3-7): p. 1049-1052.

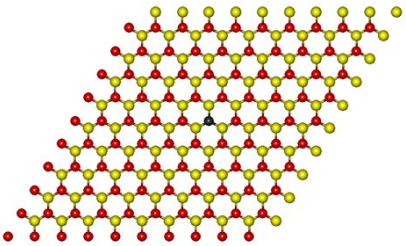

x = 0.01 ΔH_{mix} = +0.39

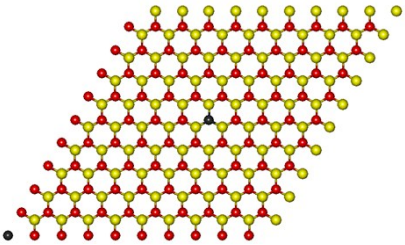

x = 0.02 ΔH_{mix} = +0.39

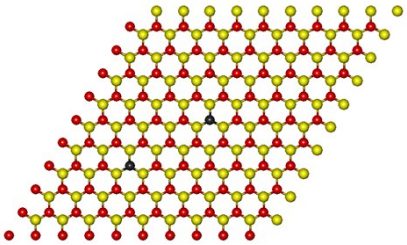

x = 0.02 ΔH_{mix} = +0.23

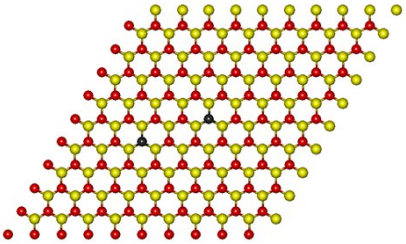

x = 0.02 ΔH_{mix} = +0.21

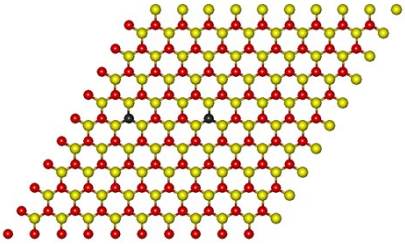

x = 0.02 ΔH_{mix} = +0.10

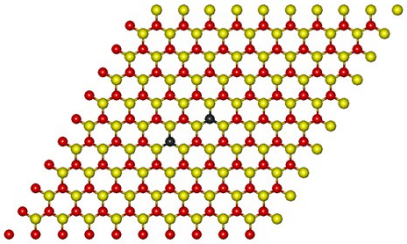

x = 0.02 ΔH_{mix} = +0.18

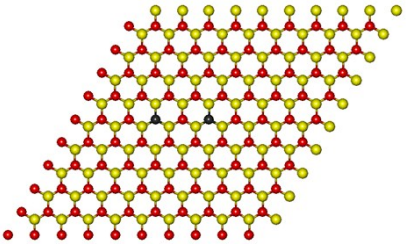

x = 0.02 ΔH_{mix} = +0.33

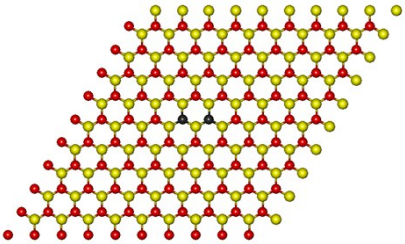

x = 0.02 ΔH_{mix} = +0.08

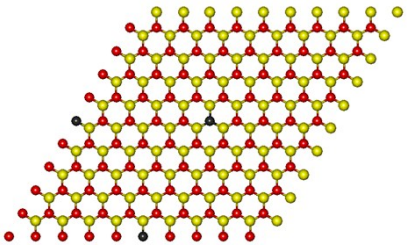

x = 0.03 ΔH_{mix} = +0.39

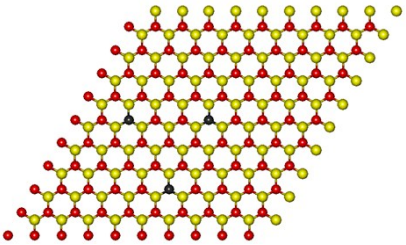

x = 0.03 ΔH_{mix} = +0.27

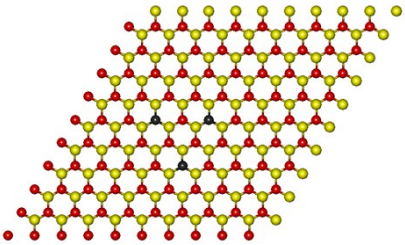

x = 0.03 ΔH_{mix} = +0.14

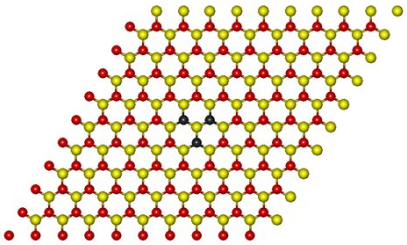

x = 0.03 ΔH_{mix} = +0.02

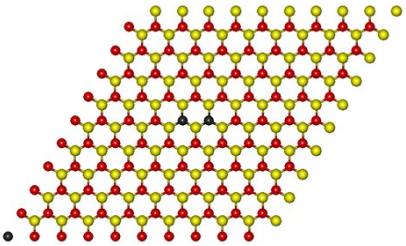

x = 0.03 ΔH_{mix} = +0.03

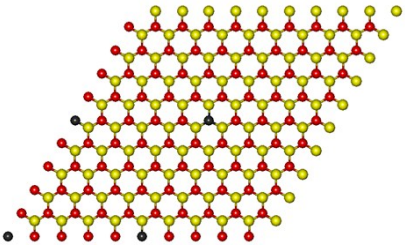

x = 0.04 ΔH_{mix} = +0.38

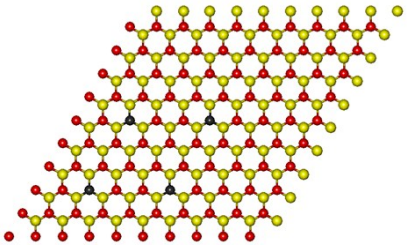

x = 0.04 ΔH_{mix} = +0.21

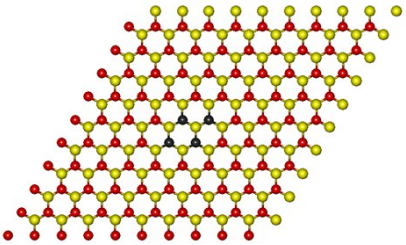

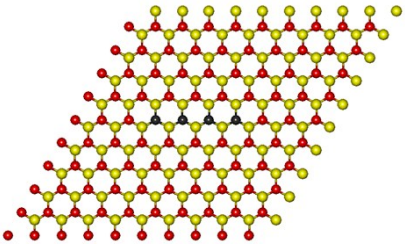

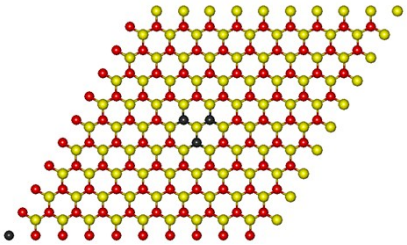

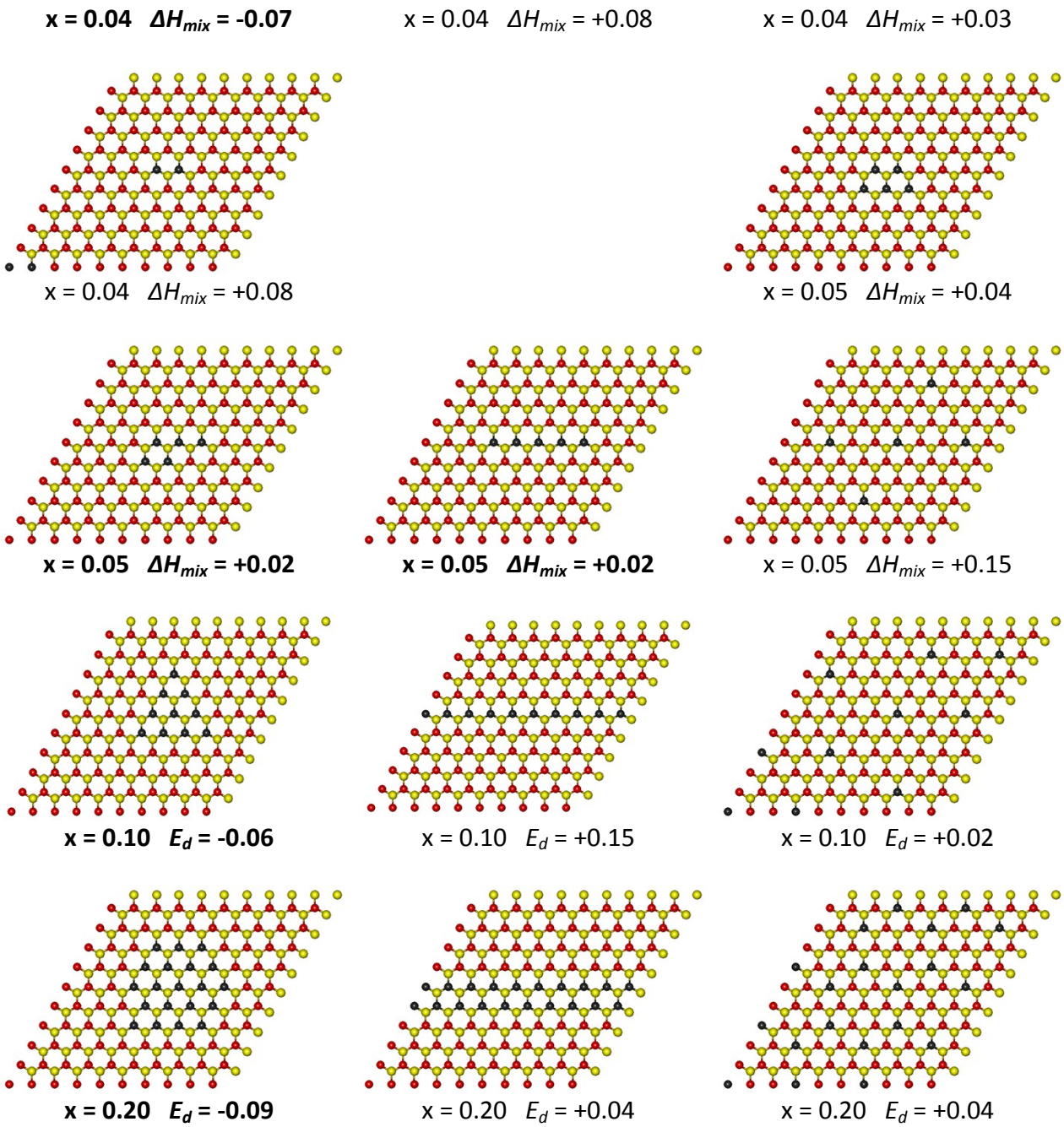

Figure S4. The formations energies ΔH_{mix} (in eV/Re-atom) for the $Mo_{1-x}Re_xS_2$ solid solutions as a function of the impurity content *x* and the distribution of impurity atoms. The results were obtained after DFTB calculations using the 10*a*×10*a* supercell of MoS_2 layer. Mo, S and Re atoms are painted in red, yellow and black, respectively.

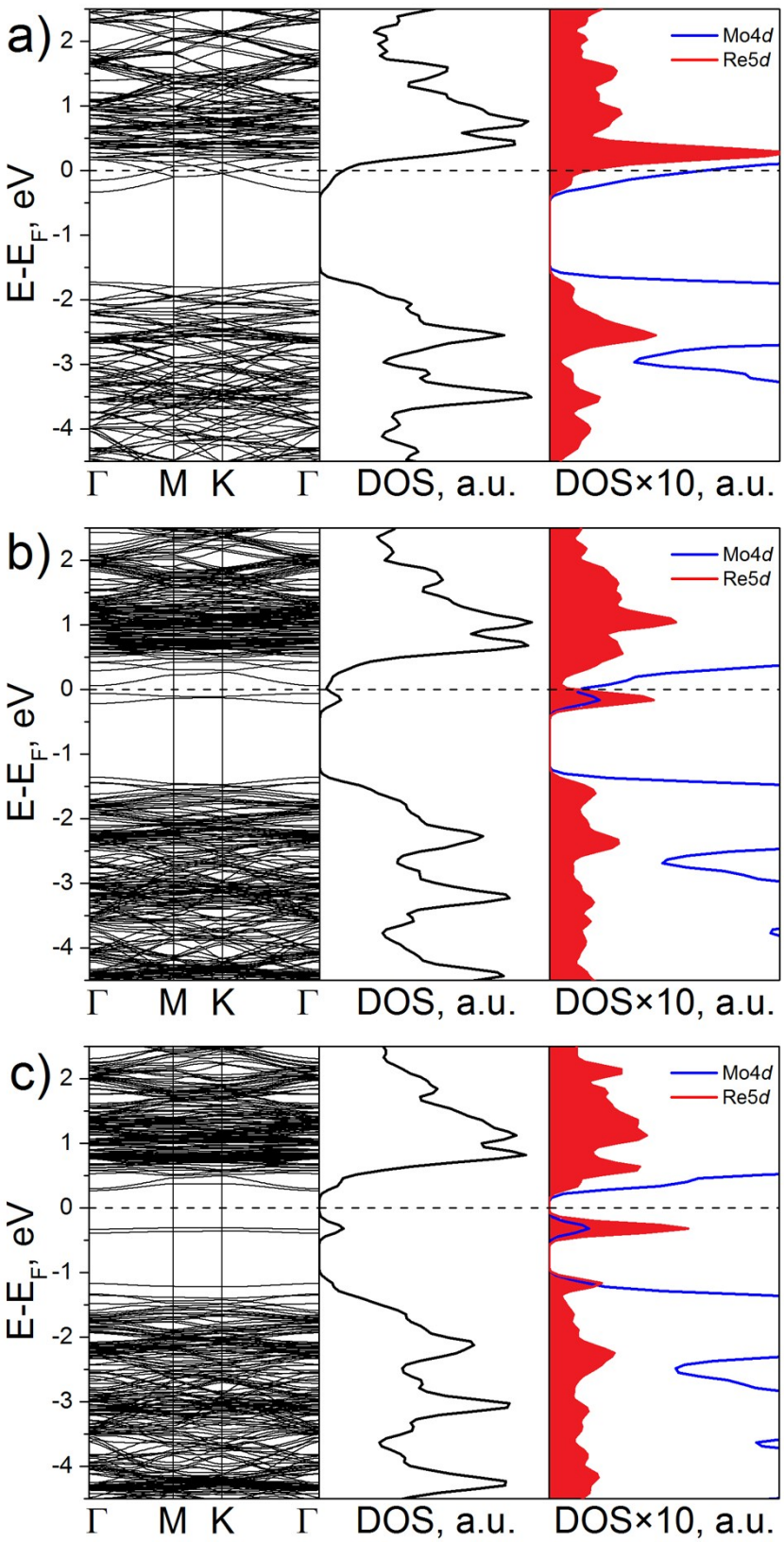

Figure S5. Band structure and densities-of-states (DOS) for the $Mo_{1-x}Re_xS_2$ (x≈0.1) solid state solutions with equidistant single Re atoms (a), with dimer-like (b) or rhombus-like cluster of Re atoms (c). Total DOS is depicted as full black line, valent Mo4*d*- and Re5*d*-states are painted in blue and red, respectively. DFT calculations.

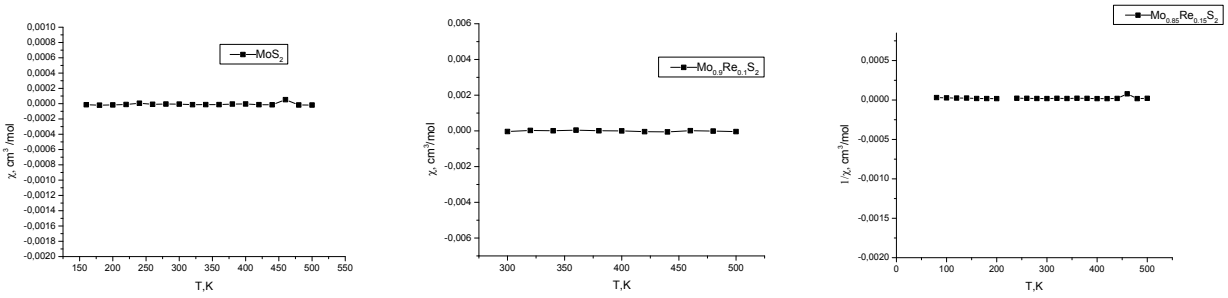

a) b) c)

Figure S6. Magnetic susceptibility of a) MoS_2, b) $Mo_{0.9}Re_{0.1}S_2$ and c) $Mo_{0.85}Re_{0.15}S_2$

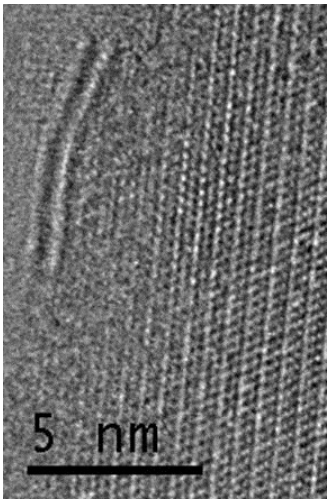

Figure S7. Nanoparticle containing two disulfide layers in contact with an edge of a wider platelet.

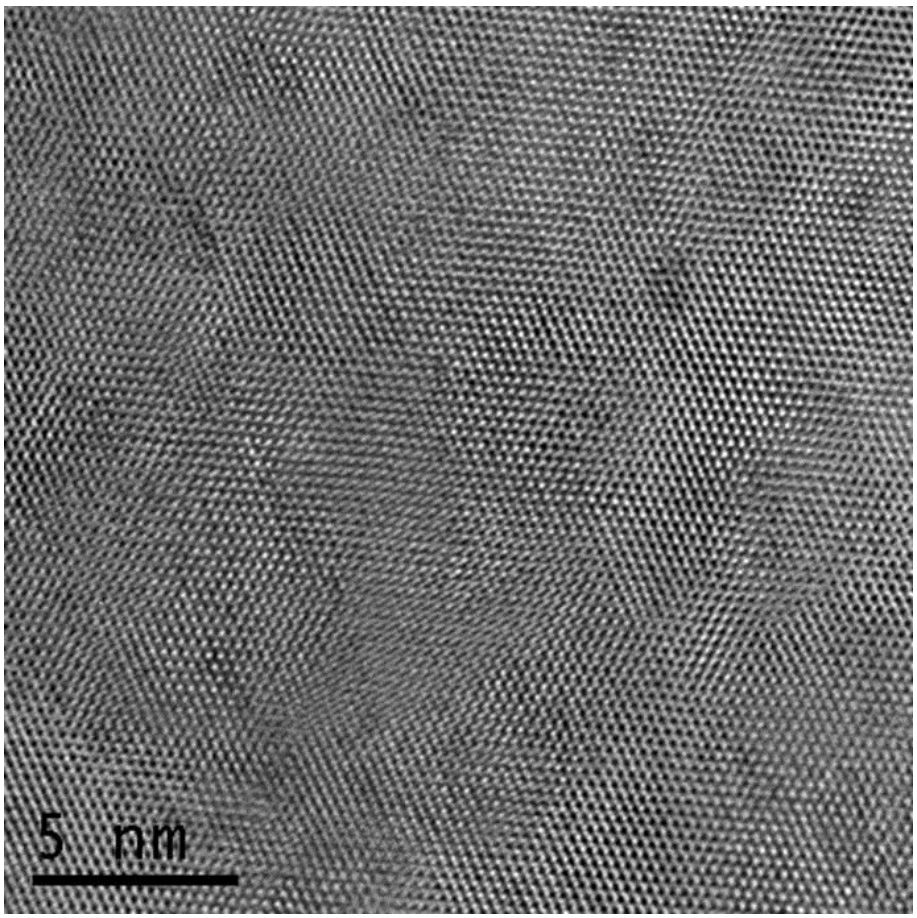

Figure S8. HRTEM-images of a thin layered particle of the $Mo_{0.85}Re_{0.15}S_2$ sample with inclusions (oriented along the [001] direction) obtained at different defocusings OL.

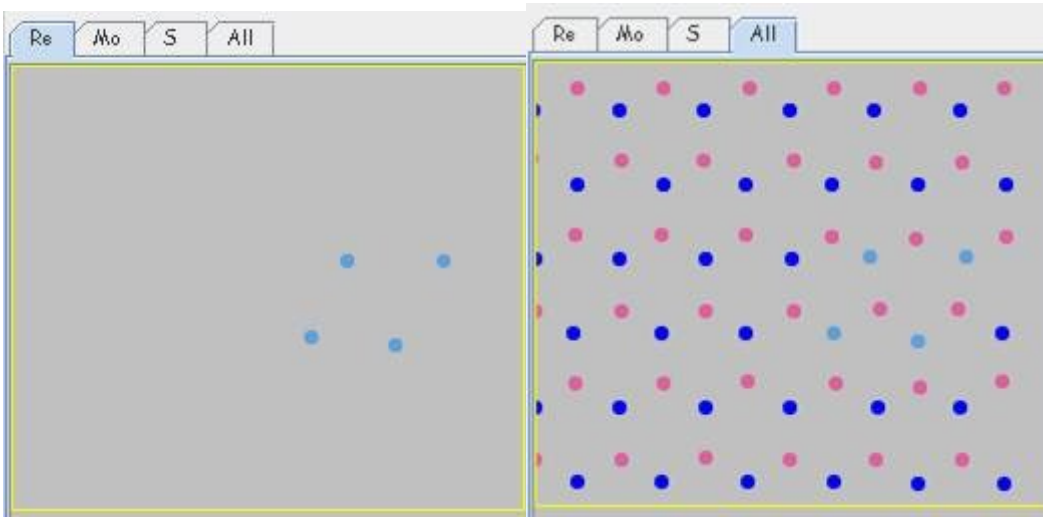

Figure S9. Schematic representation of the substitution of molybdenum with rhenium, accompanied by the formation of 4-atomic clusters ([001] projection).

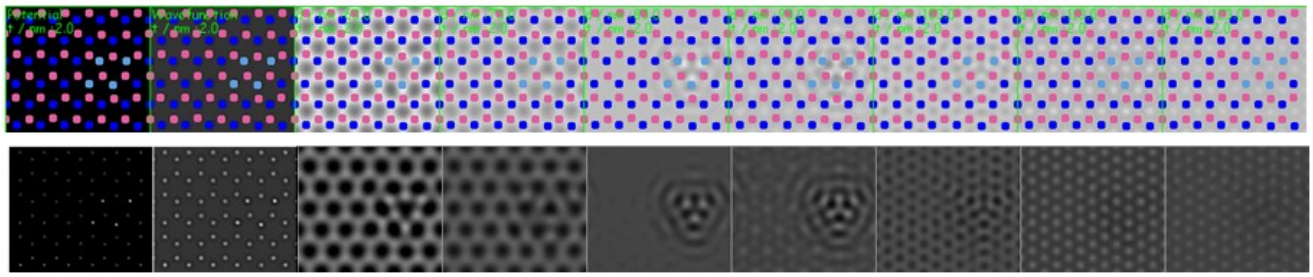

Figure S10. Series of simulated HRTEM images for a selected area for monolayer MoS_2 with 4 substituted Re atoms linked in cluster. From left to right, the Δ f changes from 43 nm to 103 nm with an increment of 10 nm.